

NEW ZZ CETI STARS FROM THE LAMOST SURVEY

JIE SU,^{1,2,*} JIANNING FU,¹ GUIFANG LIN,^{3,2,4} FANGFANG CHEN,¹
PONGSAK KHOKHUNTOD,¹ AND CHUNQIAN LI¹

¹*Department of Astronomy, Beijing Normal University, Beijing 100875, China*

²*Key Laboratory for the Structure and Evolution of Celestial Objects, Chinese Academy of Sciences*

³*Yunnan Observatories, Chinese Academy of Sciences, Kunming 650216, China*

⁴*Center for Astronomical Mega-Science, Chinese Academy of Sciences, Beijing 100012, China*

ABSTRACT

The spectroscopic sky survey carried out by the Large Sky Area Multi-Object Fiber Spectroscopic Telescope (LAMOST) provides the largest stellar spectra library in the world until now. A large number of new DA white dwarfs had been identified based on the LAMOST spectra. The effective temperature (T_{eff}) and surface gravity ($\log g$) of most DA white dwarfs were determined and published in the catalogs, e.g. Zhao et al. (2013), Rebassa-Mansergas et al. (2015), Gentile Fusillo et al. (2015) and Guo et al. (2015). We selected ZZ Ceti candidates from the published catalogs by considering whether their T_{eff} are situated in the ZZ Ceti instability strip. The follow-up time-series photometric observations for the candidates were performed in 2015 and 2016. Four stars: LAMOST J004628.31+343319.90, LAMOST J062159.49+252335.9, LAMOST J010302.46+433756.2 and LAMOST J013033.90+273757.9 are finally confirmed to be new ZZ Ceti stars. They show dominant peaks with amplitudes rising above the 99.9% confidence level in the amplitude spectra. As LAMOST J004628.31+343319.90 has an estimated mass of $\sim 0.40 M_{\odot}$ and LAMOST J013033.90+273757.9 has a mass of $\sim 0.45 M_{\odot}$ derived from their $\log g$ values, these two stars are inferred to be potential helium-core white dwarfs.

Keywords: surveys — stars: oscillations — white dwarfs

Corresponding author: Jianning Fu
jnfu@bnu.edu.cn

* LAMOST Fellow

1. INTRODUCTION

White dwarfs are the final evolutionary stage of low- and medium-mass stars. They are stellar remnants composed mostly of electron degenerate matter. The vast majority ($\sim 98\%$) of stars in the universe are expected to evolve into white dwarfs. They thus present an important boundary condition for investigating the previous evolution of stars. White dwarfs are recognized to be reliable clocks for determining the cosmic chronology, due to the simplicity of their evolution. In particular, white dwarfs are ready-made laboratories for studying physical processes under extreme conditions (Winget & Kepler 2008; Althaus et al. 2010).

There are separate instability strips of white dwarfs that associate with their atmosphere composition. More than 80% of white dwarfs are classified under the spectral type of DA, which have hydrogen-rich atmospheres. The instability strip of DA white dwarfs is located in a narrow range of effective temperature (T_{eff}) between ~ 12500 and ~ 10500 K for a typical mass of $\sim 0.6 M_{\odot}$ (Gianninas et al. 2011). As DA white dwarfs cool and pass through the corresponding instability strip, pulsations are thought to be excited by both the κ - γ mechanism due to the partial ionization of hydrogen (Dolez & Vauclair 1981; Winget et al. 1982) and the convective driving mechanism (Brickhill 1991). The pulsations in DA white dwarfs result in brightness variations with typical periods between ~ 100 and ~ 1500 s. The pulsating DA white dwarfs are known as DAV or ZZ Ceti stars.

Pulsations observed in pulsating white dwarfs are non-radial g-modes, with buoyancy as the restoring force. Different pulsating modes propagate through different regions inside a white dwarf. By detecting the pulsating modes and matching them to those of theoretical models, one can probe the invisible interior of a white dwarf to get information about its composition and internal structure, and then to determine its stellar parameters such as masses (total mass and masses of H/He layers), effective temperature, luminosity, rotation period and magnetic field strength, etc. This technique is called asteroseismology, somewhat similar to the technique that seismologists use to study the interior of the Earth using seismic waves.

Researches on ZZ Ceti stars have been carried out for decades since the discovery of the first ZZ Ceti star, HL Tau 76, by Landolt (1968). Detailed asteroseismological analyses require precise identification of pulsating modes, which requires a long interrupted high-precision observation of the targets. Conventional ground-based observations have their limitations on obtaining long continuous data. However, the barriers have been overcome by multi-site campaigns, especially through the Whole Earth Telescope (Nather et al. 1990) or by space mission such as *Kepler* (Borucki et al. 2010). On the other hand, comprehensive asteroseismological research requires a large sample of pulsating white dwarfs. In order to enlarge the sample, searching for new pulsating white dwarfs is necessary.

The Large Sky Area Multi-Object Fiber Spectroscopic Telescope (LAMOST, also called Guoshoujing Telescope), as one of the National Major Scientific Projects un-

dertaken by the Chinese Academy of Science, is located in Xinglong Observatory of National Astronomical Observatories, Chinese Academy of Sciences. It is a special quasi-meridian reflecting Schmidt telescope with 4000 fibers in a field of view (FOV) of $5^\circ \times 5^\circ$, which guarantees a high efficiency of acquiring spectra (Cui et al. 2012). The spectroscopic sky survey carried out by LAMOST has been running since 2011. The pilot survey was launched in October, 2011 and ended in June, 2012 (Zhao et al. 2012; Luo et al. 2012). A five-year regular survey, which was initiated in September, 2012 and terminated in June, 2017. In the past five years of survey, a total number of 7664073 spectra (the fourth data release, DR4, including 6856896 stars, 118657 galaxies, 36374 quasars and 652146 other unknown objects) have been obtained, which offer the largest stellar spectra library in the world until now.

A large number of white dwarfs including those of hydrogen-rich atmospheres, helium-rich atmospheres and white dwarf-main sequence binaries had been spectroscopically identified based on the LAMOST spectra (see the catalogs published by Zhao et al. 2013; Zhang et al. 2013; Ren et al. 2013, 2014; Rebassa-Mansergas et al. 2015; Gentile Fusillo et al. 2015; Guo et al. 2015). Most of them are new sources, which further expand the number of known white dwarfs. This provides opportunities to search for new pulsating white dwarfs. The spectral types of the sources can be determined based on the spectra and the atmospheric parameters (T_{eff} and $\log g$) of most DA white dwarfs are derived and provided along with the catalogs.

We selected DA white dwarfs whose effective temperatures meet the condition of $10000 \leq T_{\text{eff}} \pm \sigma \leq 14000$ K as the ZZ Ceti candidates. Here σ is the error of T_{eff} given in the catalogs. The typical value (median) of σ is 458 K. Note that, we had set a less rigorous criterion for selecting candidates concerning the errors of T_{eff} and to avoid missing some potential targets. The temperature range of the criterion is wider than the empirical ZZ Ceti instability strip, regardless of $\log g$, although the instability strip position seems to be $\log g$ and T_{eff} dependent. We then perform time-series photometry on individual candidate to ascertain whether pulsations are detected.

In this paper, we report the progress of our search for new pulsating white dwarfs. Four new ZZ Ceti stars have been photometrically confirmed in 2015 and 2016, which are LAMOST J004628.31+343319.90 (hereafter J004628), LAMOST J062159.49+252335.9 (hereafter J062159), LAMOST J010302.46+433756.2 (hereafter J010302) and LAMOST J013033.90+273757.9 (hereafter J013033). The LAMOST spectra and stellar parameters of the four new ZZ Ceti stars are described in Section 2. In Section 3, we summarize the observations, data reduction and pulsation analysis. In Section 4, the significance criteria are discussed. Discussion and conclusions are in Section 5.

2. LAMOST SPECTRA AND STELLAR PARAMETERS

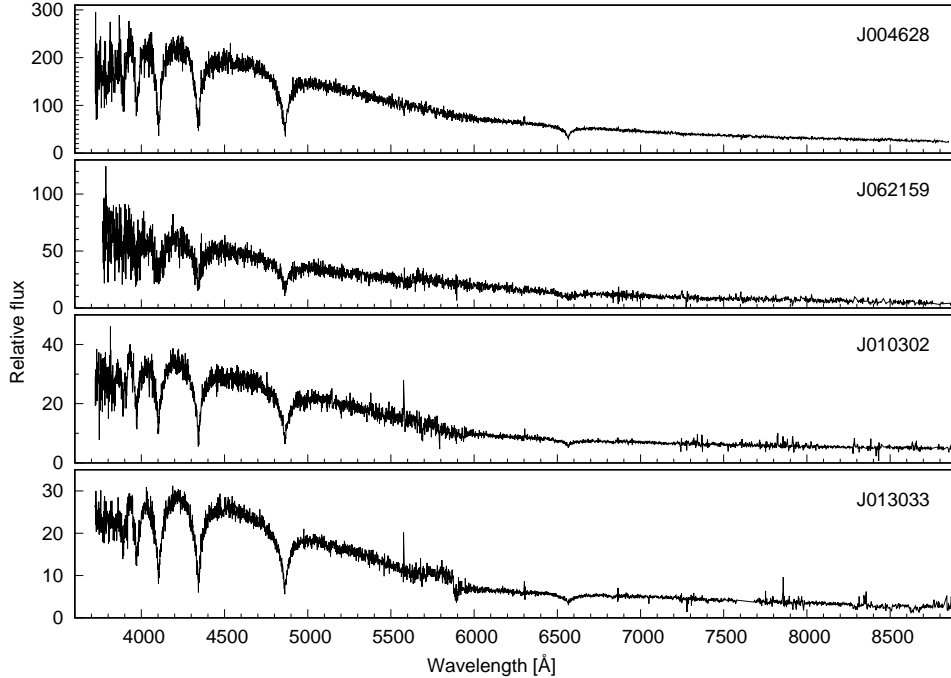


Figure 1. The LAMOST spectra of the four white dwarfs.

Table 1. Summary of information about the LAMOST spectra.

Object	RA (deg)	Dec. (deg)	Obs. Date	Plan ID	Sp. ID	Fiber ID	S/N _g
J004628	11.61796	+34.55553	2011-12-11	M31_007N34_B1	3	9	10.89
J062159	95.49792	+25.39331	2013-01-11	GAC094N27M1	7	21	6.76
J010302	15.76029	+43.63228	2013-12-29	M31016N43M1	3	154	8.36
J013033	22.64129	+27.63275	2014-01-01	M31023N28M1	3	245	12.63

Figure 1 shows the flux- and wavelength-calibrated, sky-subtracted spectra of the four new ZZ Ceti stars, which are obtained from the LAMOST database ¹. The information about these spectra is summarized in Table 1. Columns 1 to 4 list the name, coordinates (J2000) and date of observations of each star. Columns 5 to 7 list the identifiers of plan, spectrograph and fiber of the spectra. Column 8 lists the signal-to-noise ratio (S/N) in *g* band of each individual spectrum.

The apparent magnitudes and stellar parameters of the four new ZZ Ceti stars are listed in Table 2. Column 1 is the name of object. Columns 2 to 6 list the apparent magnitudes of each star. The atmospheric parameters T_{eff} and $\log g$ are listed in

¹ <http://dr4.lamost.org/>

Table 2. Apparent magnitude and stellar parameters of the four new ZZ Ceti stars.

Object	Apparent magnitude					T_{eff} (K)	$\log g$ (cgs)	Mass (M_{\odot})	References
	u	g	r	i	z				
J004628	16.83	16.33	16.40	16.53	16.75	14644 (808)	7.60 (0.18)	0.41 (0.08)	1
						11681 (199)	7.53 (0.15)	0.38 (0.05)	4
J062159	-	17.56	17.62	17.70	-	11728 (651)	8.25 (0.31)	0.76 (0.19)	2
J010302	18.84	18.33	18.43	18.57	18.72	11750 (492)	7.89 (0.33)	0.54 (0.21)	3
J013033	18.99	18.57	18.70	18.85	19.03	14127 (334)	7.69 (0.07)	0.45 (0.03)	4

NOTE—References: (1) [Zhao et al. 2013](#); (2) [Rebassa-Mansergas et al. 2015](#); (3) [Gentile Fusillo et al. 2015](#); (4) [Guo et al. 2015](#)

columns 7 and 8. The mass estimated according to the atmospheric parameters is listed in column 9. The last column indicates the source of the parameters.

We note that there are two sets of parameters of J004628, which are derived from catalogs of [Zhao et al. \(2013\)](#) and [Guo et al. \(2015\)](#), respectively. The values of $\log g$ from the two catalogs are compatible to each other, but the values of T_{eff} are quite different. However, both T_{eff} meet our selecting criterion (see Section 1). We like to point out that there is a large uncertainty in the determination of the value of T_{eff} of this star.

3. OBSERVATIONS AND DATA ANALYSIS

3.1. Observations

As the ZZ Ceti stars are relatively faint, the observations were performed with the two 2 m-class telescopes in China: the 2.4-m telescope (LJ 240, [Fan et al. 2015](#)) at the Lijiang Observatory of Yunnan Observatories, Chinese Academy of Sciences (YNAO) and the 2.16-m telescope (XL 216, [Fan et al. 2016](#)) at the Xinglong Observatory of National Astronomical Observatories, Chinese Academy of Sciences (NAOC). The journal of observation is summarized in Table 3.

J004628 and J062159 were observed with LJ 240 on 2015 January 27 and 2016 January 17, respectively. Images of J004628 were taken with a Princeton Instruments VersArray:1300B back-illuminated CCD Camera, which has the CCD size of 1300×1340 with the FOV of $4.40' \times 4.48'$. The exposure time was set as 40 s for each image. Images of J062159 were obtained with another instrument, the Yunnan Faint Object Spectrograph and Camera (YFOOSC), which has the CCD size of 2048×2048 and the FOV of $9.6' \times 9.6'$ under the direct imaging mode. The exposure time of each image was 50 s. No filter was used during the above observations in order to obtain as many photons as possible.

Table 3. Journal of observations for the new ZZ Ceti stars.

Object	Obs. Date	Telescope	Start Time (HJD)	End Time (HJD)	Length (h)	Exp. Time (s)
J004628	2015-01-27	LJ 240	2457050.0347	2457050.1209	2.07	40
J062159	2016-01-17		2457404.9884	2457405.1627	4.18	50
J010302	2016-11-26	XL 216	2457718.9322	2457719.0453	2.71	60
J013033	2016-11-27		2457719.9357	2457720.0457	2.64	70

J010302 and J013033 were observed with XL 216 on 2016 November 26 and 27, respectively. The YFOSC’s sister instrument, the Beijing Faint Object Spectrograph and Camera (BFOSC) was used, which has the CCD size of 2048×2048 and the FOV of $9.36' \times 9.36'$ under the direct imaging mode. The exposure time of each image was 60s for J010302 and 70s for J013033, respectively. No filter was used during the observations.

3.2. Data Reduction

All the observed data were reduced using the IRAF² packages. The instrumental magnitudes of stars on each image were calculated by using the method of aperture photometry according to the standard procedure. The differential magnitude of the candidate star relative to the comparison star was calculated and plotted versus the time of observation to produce the light curve. In order to get rid of the low-frequency variations of the atmospheric transparency during the night, the light curves were divided by a fourth order polynomial. The normalized light curves of the four stars are shown in the upper panels of Figure 2 to Figure 5. Periodical variations are clearly visible in the light curves.

3.3. Fourier Analysis

In order to further verify the variability of these stars, we performed discrete Fourier transform (DFT) of the light curves to search for periodical variations. The amplitude spectra of the light curves are shown in the bottom panels of Figure 2 to Figure 5. The spectral window corresponding to each light curve is shown in the inset. The spectral window (or window function) is the DFT of a single period sinusoidal function sampled as the data, whose value equals to unity at each data point and zero elsewhere. It reflects the effect of spectral leakage due to finite time duration and gaps in the light curve. In the ideal case (an infinite duration signal), it will be a δ function. In reality,

² IRAF is distributed by the National Optical Astronomy Observatories, which are operated by the Association of Universities for Research in Astronomy, Inc., under cooperative agreement with the National Science Foundation.

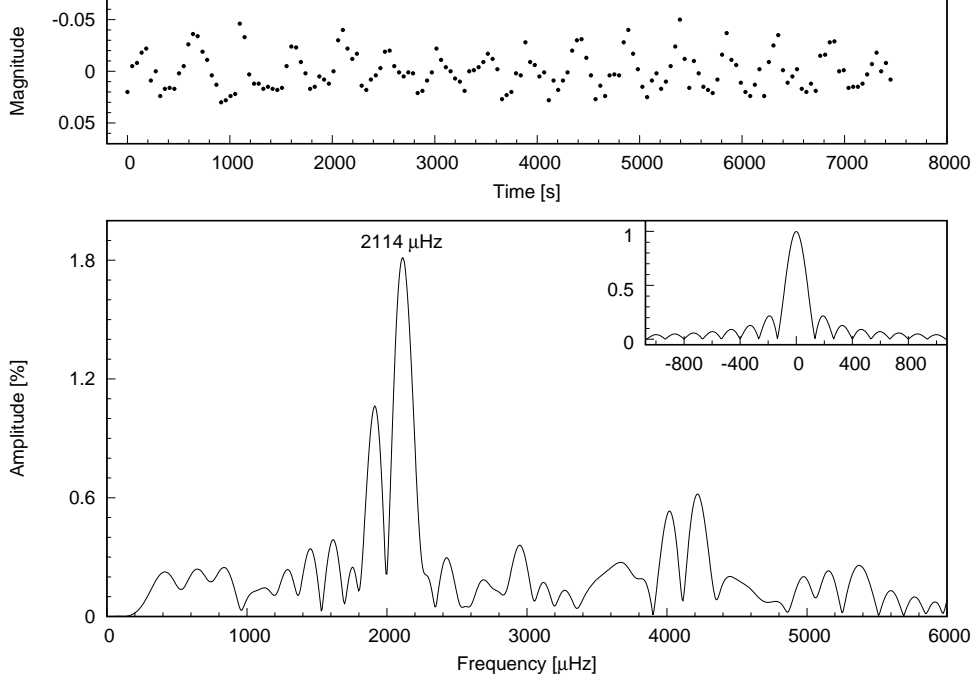


Figure 2. The upper panel shows the normalized light curve of J004628. The x -axis is the time in second and the y -axis the differential magnitude of J004628 relative to the comparison star. The zero point is the average of the light curve. The bottom panel shows the amplitude spectrum of the light curve. The relative amplitude is plotted versus the frequency in the range from 0 to 6000 μHz . The inset shows the spectral window.

it will far from the δ function and helps us identify the actual modes from aliases due to imperfect sampling.

Figure 2 shows the amplitude spectrum of J004628. The highest peak with an amplitude of 1.8% is detected at the frequency of $2114 \pm 12 \mu\text{Hz}$ (the period of $473 \pm 3 \text{s}$). Figure 3 shows the case of J062159. The highest peak is located at the frequency of $1205 \pm 6 \mu\text{Hz}$ (the period of $830 \pm 4 \text{s}$) with an amplitude of 1.9%. The amplitude spectrum of J010302 is shown in Figure 4 with a dominant peak at the frequency of $852 \pm 10 \mu\text{Hz}$ (the period of $1174 \pm 14 \text{s}$), which has an amplitude of 1.7%. In the amplitude spectrum of J013033 shown in Figure 5, a dominant peak with an amplitude of 1.5% is found at the frequency of $3228 \pm 14 \mu\text{Hz}$ (the period of $310 \pm 1 \text{s}$). The uncertainties of frequencies are estimated by using Monte Carlo simulations as described in Fu et al. (2013) and applied in our previous work (Su et al. 2014a,b).

4. SIGNIFICANCE CRITERIA

In order to give quantitative criteria to determine whether the dominant peaks are significant or not, we simulated light curves to estimate the significance thresholds for each star. The simulations are based on the principle described in Greiss et al. (2014, 2016). In summary, we keep the time of data points of the original light curve in place, but randomly permute brightness to create a simulated light curve. We then perform DFT on each simulated light curve and record the highest amplitude in the

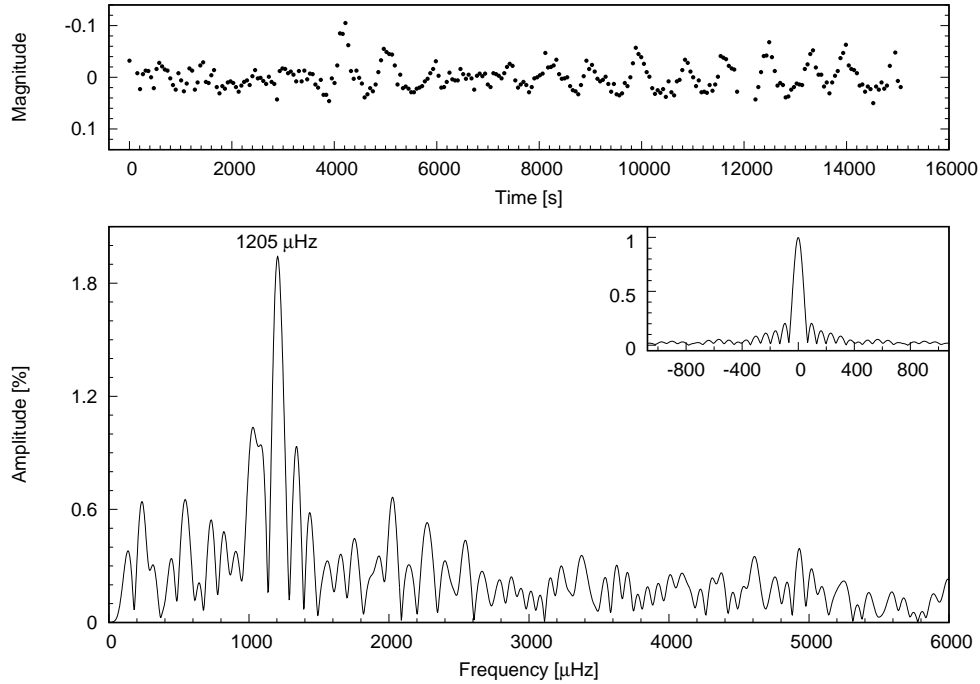


Figure 3. Same as Figure 2 but for J062159.

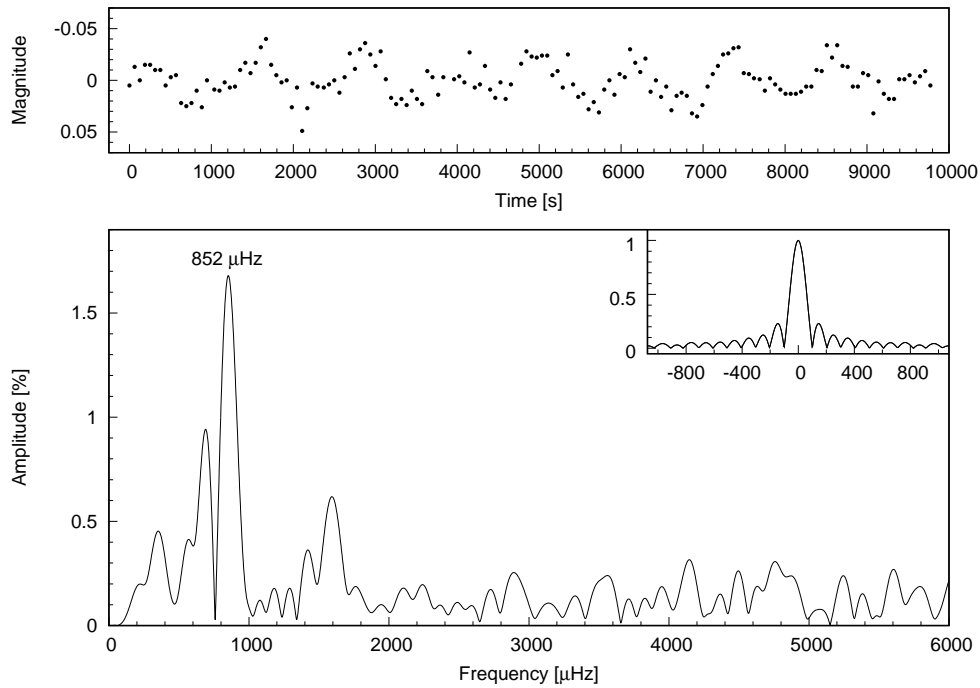


Figure 4. Same as Figure 2 but for J010302.

amplitude spectrum. This operation is repeated 10000 times. All of the recorded highest amplitudes thus constitute a random sample. The cumulative distribution function (CDF) of the sample is calculated. The value of the CDF at any particular value of x , denoted by $F(x)$, is the fraction of the elements in the sample that are less

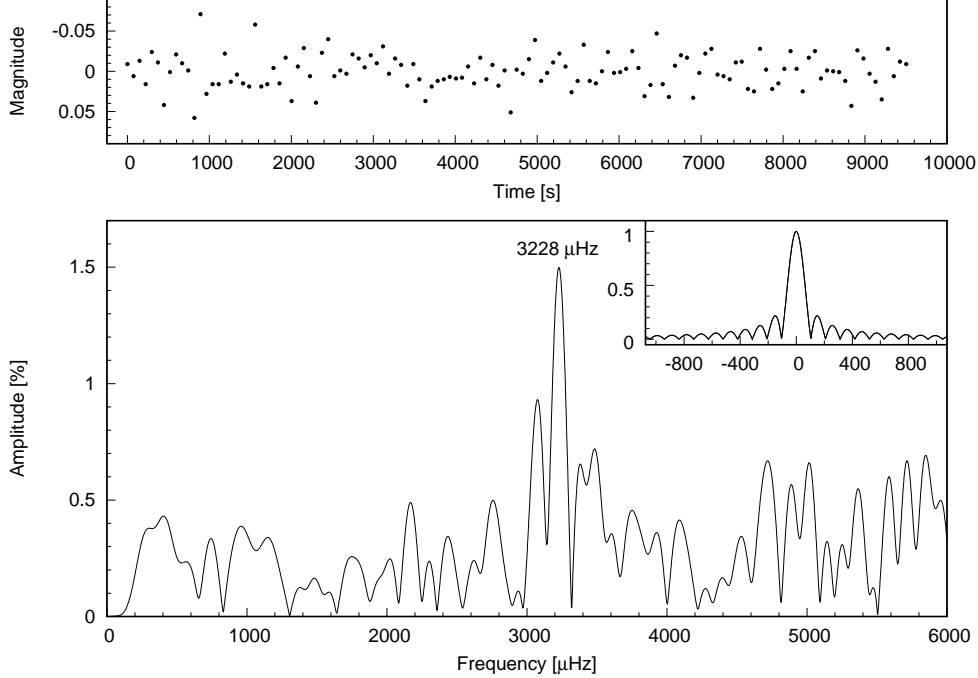


Figure 5. Same as Figure 2 but for J013033.

than or equal to x . The values at the 95th, 99th and 99.9th percentiles, which means that 95%, 99% and 99.9% of the simulated light curves have the highest amplitudes fall below those values, are determined from the CDF and taken as significance criteria (confidence levels).

We generate 10000 simulated light curves for each star. Our previous experience showed that the results converged well using 10000 simulated light curves. The distribution of the recorded highest amplitudes in the simulated sample of each star is shown as a histogram in the upper panel of each sub-figure of Figure 6. To construct the histogram, the entire range of each sample is divided into a series of intervals (bins), here the bin width is 0.01%. The y -axis indicates the number of values fall into each bin. The bottom panel of each sub-figure shows the CDF calculated based on the distribution. The locations of the 95%, 99% and 99.9% confidence levels are marked with the dashed, dotted and dash-dotted lines, respectively.

Figure 7 shows amplitude spectra with confidence levels of the four stars. The 95%, 99% and 99.9% confidence levels are marked with the dashed, dotted and dash-dotted lines respectively in each amplitude spectrum. The $4\langle A \rangle$ level, which is a widespread used significance criterion (Breger et al. 1993; Kuschnig et al. 1997), is also marked with the solid line for comparison. Here, we take the average amplitude ($\langle A \rangle$) of the amplitude spectrum as an estimate of the noise level.

The 99.9% confidence level corresponds to a more strict significance threshold than the 3σ level. All the highest peaks in the four amplitude spectra rise above the 99.9% confidence levels. They are thus considered significant. In addition, another significant peak at frequency $\approx 1913 \mu\text{Hz}$ (period $\approx 523 \text{ s}$) is found in the amplitude

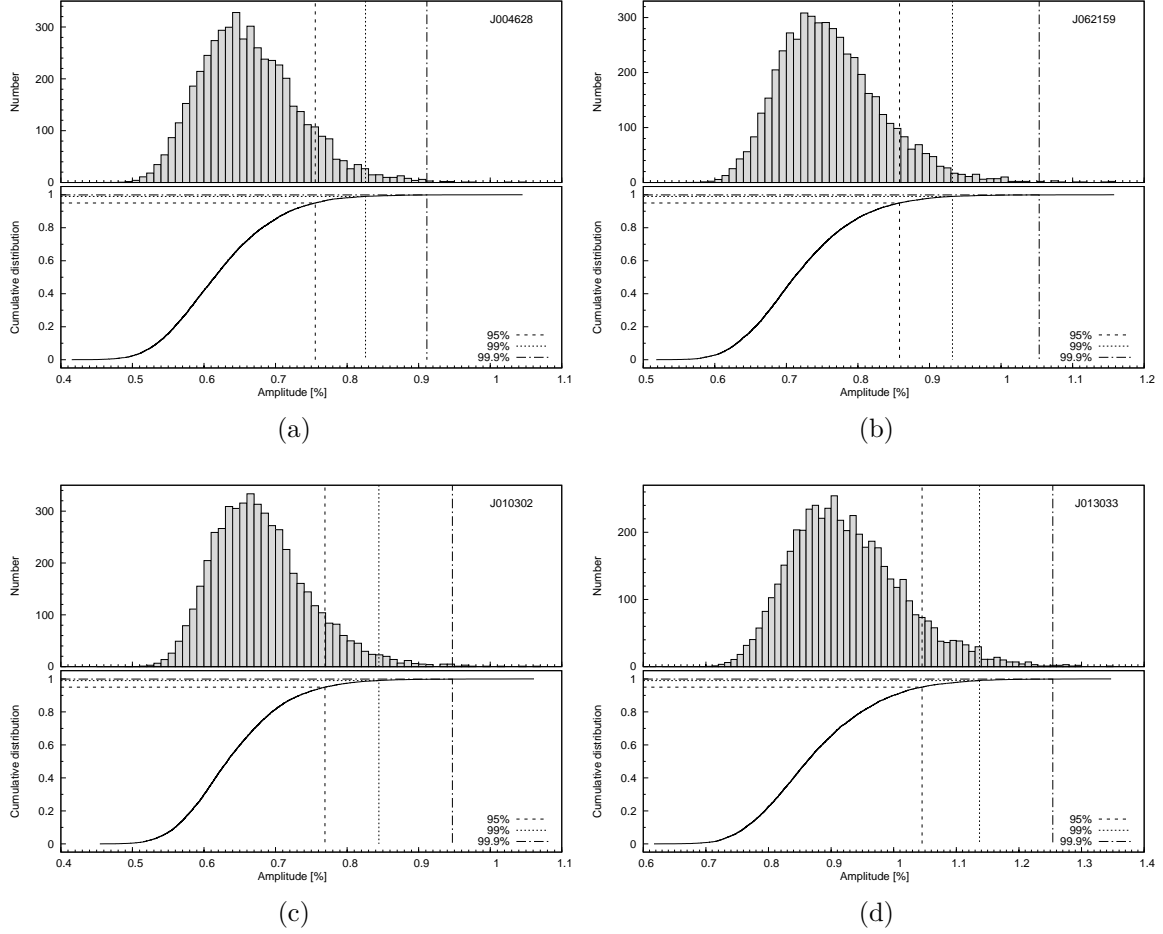


Figure 6. The simulation results for (a) J004628, (b) J062159, (c) J010302 and (d) J013033. The upper panel of each sub-figure shows the distribution of the highest amplitudes in 10000 simulations. The bottom panel shows the corresponding CDF. The locations of the 95%, 99% and 99.9% confidence levels are marked with the dashed, dotted and dash-dotted lines, respectively.

spectrum of J004628. In order to check the significance of the second peak, we prewhiten the original light curve of J004628 with the highest peak and perform simulations based on the residual light curve to estimate the confidence levels. The residual amplitude spectrum and confidence levels are shown in Figure 7(e). The original amplitude spectrum is plotted with the dotted lines for comparison. The second peak is still significant.

Meanwhile, we note that the $4\langle A \rangle$ levels in all amplitude spectra are above the 95% confidence levels. If we roughly take the $4\langle A \rangle$ level as the significance threshold, any peak whose amplitude exceeds that threshold can be considered significant in a sufficient confidence level higher than 95%.

5. DISCUSSION AND CONCLUSIONS

Four new ZZ Ceti stars have been identified. All of them are selected from the LAMOST spectroscopic survey dataset and confirmed by the follow-up photomet-

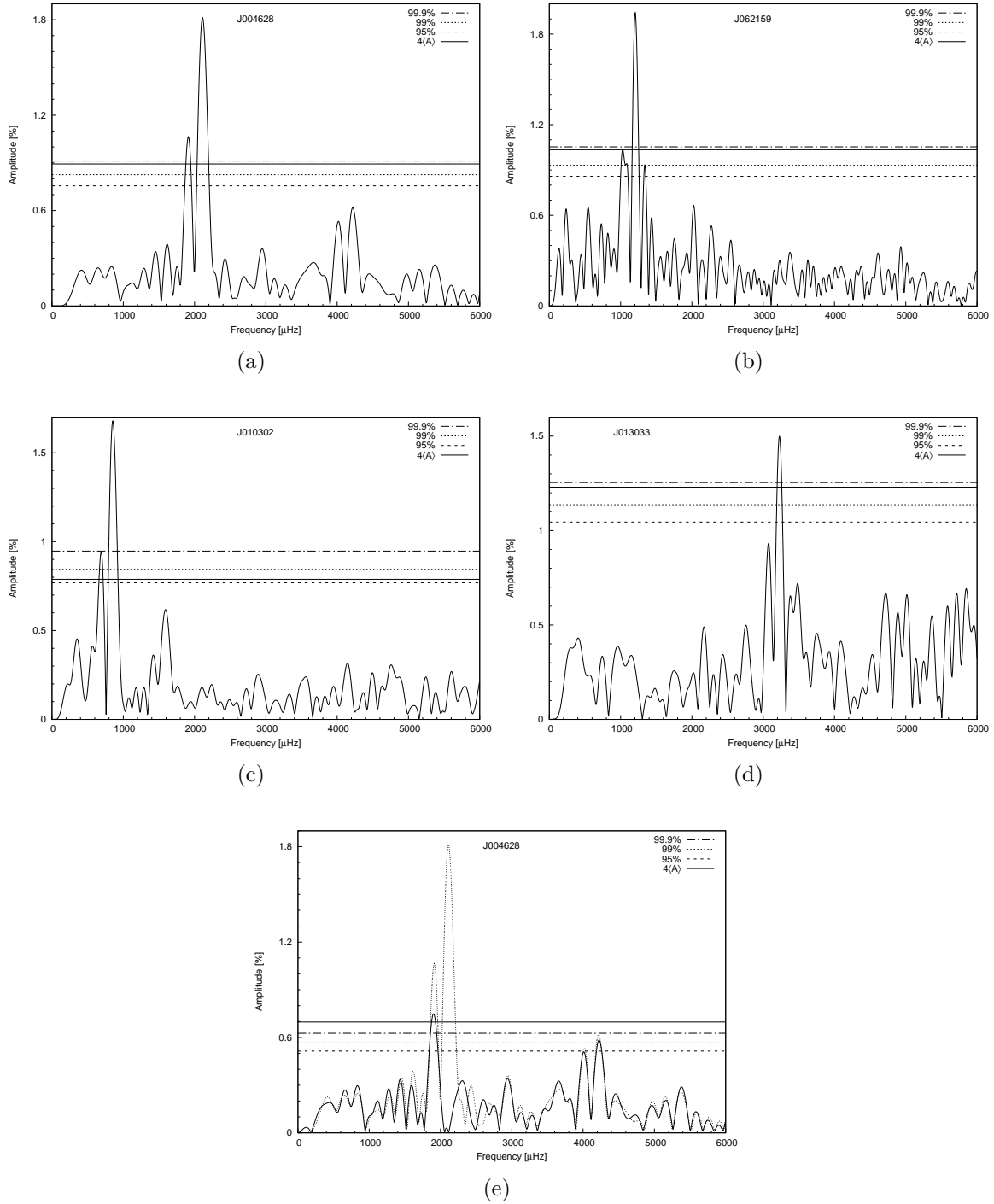


Figure 7. Amplitude spectra with confidence levels of the new ZZ Ceti stars: (a) J004628, (b) J062159, (c) J010302, (d) J013033 and (e) the case for J004628 after prewhitening with the highest peak. The 95%, 99% and 99.9% confidence levels and the $4\langle A \rangle$ levels are marked with the dashed, dotted, dash-dotted and solid lines, respectively.

ric observations. Figure 8 shows the $T_{\text{eff}}\text{-}\log g$ diagram of 172 known ZZ Ceti stars with determined atmospheric parameters. These known objects were collected from the literature (14 from Kepler et al. (2005), 41 from Mukadam et al. (2006), 5 from Voss et al. (2006, 2007), 34 from Castanheira et al. (2006, 2007, 2010, 2013), 56 from Gianninas et al. (2011), 6 from Green et al. (2015), 11 in the *Kepler* field (Hermes et al. 2011; Greiss et al. 2014, 2016) and 5 massive or ultramassive ZZ Ceti stars discovered by Hermes et al. (2013) and Curd et al. (2017)). The positions of our new ZZ Ceti stars are marked in the diagram with the squares with error bars. The empirical boundaries of the ZZ Ceti instability strip determined by Tremblay et al. (2015) are marked with the dashed lines. J004628 had been given two different sets of atmospheric parameters, which correspond to different positions marked with the open squares in the $T_{\text{eff}}\text{-}\log g$ diagram. Obviously, the T_{eff} and $\log g$ provided by Zhao et al. (2013) place the object well outside the instability strip, while the parameters given by Guo et al. (2015) place it within the instability strip. We therefore believe that the atmospheric parameters given by the latter are more reliable. The positions of the rest three new ZZ Ceti stars in the $T_{\text{eff}}\text{-}\log g$ diagram are marked with the filled squares. J013033 had been determined with a relatively high T_{eff} and low $\log g$, which make its position seriously deviate from the instability strip. However, J013033 has the smallest error of $\log g$ among the four ZZ Ceti stars. It seems that the determination of T_{eff} about J013033 is probably not correct but the $\log g$ value would be reliable. For J062159 and J010302, their positions in the $T_{\text{eff}}\text{-}\log g$ diagram are consistent with that of ZZ Ceti stars.

Both parameter estimates for J004628 implies relatively low $\log g$ hence an estimated mass of $\sim 0.40 M_{\odot}$. The theory of stellar evolution shows that a white dwarfs whose mass $\lesssim 0.5 M_{\odot}$ cannot have a carbon-oxygen core, since the core mass is lower than the critical value for igniting helium. J004628 is hence inferred to be a white dwarf with helium core. If we believe the $\log g$ estimate of J013033, the mass of J013033 is $\sim 0.45 M_{\odot}$. Owing to the low mass of J013033, it is also inferred to be another potential helium-core white dwarf. The formation of low-mass helium-core white dwarfs requires a mechanism different from the normal single star evolution, since a single star with such low mass would take a time longer than the age of the universe to evolve into white dwarf. It is widely accepted that low-mass white dwarfs should originate from the evolution of close binary systems. The interaction between binary stars removes most of outer envelope of one component before helium ignition. The remnant of the component with a helium core would not go through the asymptotic giant branch phase and directly contracts toward a white dwarf. On the other hand, the existence of single low-mass white dwarfs and the potential formation channels for them are discussed by Brown et al. (2011). The existing observations, both light curves and spectra, temporarily cannot reveal either J004628 or J013033 has a companion. It is still open to question that the two white dwarfs are singles or not. Perhaps some objects might benefit from higher S/N spectra.

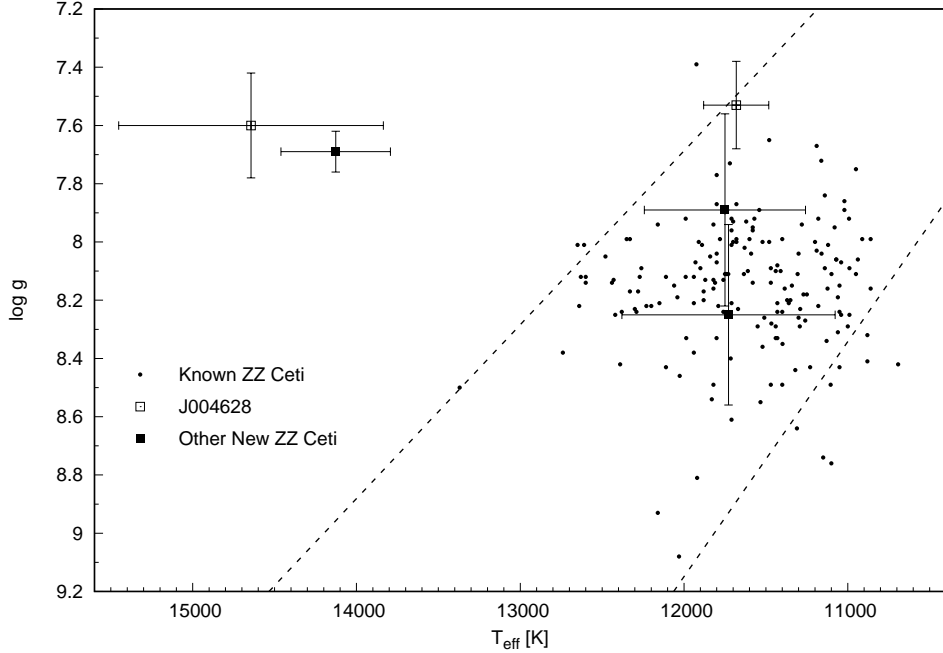


Figure 8. $T_{\text{eff}}\text{-log } g$ diagram of ZZ Ceti stars. The black points correspond to the 172 known ZZ Ceti stars with determined atmospheric parameters. The open squares with error bars mark the two positions of J004628 with different atmospheric parameters and the filled squares with error bars correspond to the rest three new ZZ Ceti stars. The empirical boundaries of the ZZ Ceti instability strip are marked with the dashed lines.

Further time-series photometric observations are needed to detect additional pulsating modes for the asteroseismological analysis, which would allow the essential parameters of the new ZZ Ceti stars to be refined. Our work of searching for new pulsating white dwarfs will continue.

We would like to thank an anonymous referee for reviewing and offering valuable comments, which greatly help us to improve the manuscript. J.S. acknowledges the support from the China Postdoctoral Science Foundation (Grant No. 2015M570960) and the foundation of Key Laboratory for the Structure and Evolution of Celestial Objects, Chinese Academy of Sciences (Grant No. OP201406). J.N.F. acknowledges the support from the National Natural Science Foundation of China (NSFC) through the grant 11673003 and the National Basic Research Program of China (973 Program 2014CB845700 and 2013CB834900). G.F.L. acknowledges the support from the NSFC under Grant No. 11503079. Fruitful discussions with Xianfei Zhang and Chun Li are greatly appreciated.

This work uses the data from the Guoshoujing Telescope (the Large Sky Area Multi-Object Fiber Spectroscopic Telescope LAMOST), which is a National Major Scientific Project built by the Chinese Academy of Sciences. Funding for the project has been provided by the National Development and Reform Commission. LAMOST is operated and managed by the National Astronomical Observatories, Chinese Academy

of Sciences. We acknowledge the support of the staff of the Lijiang 2.4m telescope. Funding for the telescope has been provided by Chinese Academy of Sciences and the People's Government of Yunnan Province. We acknowledge the support of the staff of the Xinglong 2.16m telescope. This work was partially supported by the Open Project Program of the Key Laboratory of Optical Astronomy, National Astronomical Observatories, Chinese Academy of Sciences.

Facilities: LAMOST, NOAC:2.16-m, YNAO:2.4-m

Software: IRAF

REFERENCES

- Althaus, L. G., Córscico, A. H., Isern, J., & García-Berro, E. 2010, *A&A Rv*, 18, 471
- Borucki, W. J., Koch, D., Basri, G., et al. 2010, *Science*, 327, 977
- Breger, M., Stich, J., Garrido, R., et al. 1993, *A&A*, 271, 482
- Brickhill, A. J. 1991, *MNRAS*, 251, 673
- Brown, J. M., Kilic, M., Brown, W. R., & Kenyon, S. J. 2011, *ApJ*, 730, 67
- Castanheira, B. G., Kepler, S. O., Mullally, F., et al. 2006, *A&A*, 450, 227
- Castanheira, B. G., Kepler, S. O., Costa, A. F. M., et al. 2007, *A&A*, 462, 989
- Castanheira, B. G., Kepler, S. O., Kleinman, S. J., Nitta, A., & Fraga, L. 2010, *MNRAS*, 405, 2561
- Castanheira, B. G., Kepler, S. O., Kleinman, S. J., Nitta, A., & Fraga, L. 2013, *MNRAS*, 430, 50
- Cui, X.-Q., Zhao, Y.-H., Chu, Y.-Q., et al. 2012, *RAA*, 12, 1197
- Curd, B., Gianninas, A., Bell, K. J., et al. 2017, *MNRAS*, 468, 239
- Dolez, N., & Vauclair, G. 1981, *A&A*, 102, 375
- Fan, Y.-F., Bai, J.-M., Zhang, J.-J., et al. 2015, *RAA*, 15, 918
- Fan, Z., Wang, H., Jiang, X., et al. 2016, *PASP*, 128, 115005
- Fu, J.-N., Dolez, N., Vauclair, G., et al. 2013, *MNRAS*, 429, 1585
- Gentile Fusillo, N. P., Rebassa-Mansergas, A., Gänsicke, B. T., et al. 2015, *MNRAS*, 452, 765
- Gianninas, A., Bergeron, P., & Ruiz, M. T. 2011, *ApJ*, 743, 138
- Green, E. M., Limoges, M.-M., Gianninas, A., et al. 2015, 19th European Workshop on White Dwarfs, 493, 237
- Greiss, S., Gänsicke, B. T., Hermes, J. J., et al. 2014, *MNRAS*, 438, 3086
- Greiss, S., Hermes, J. J., Gänsicke, B. T., et al. 2016, *MNRAS*, 457, 2855
- Guo, J., Zhao, J., Tziamtzis, A., et al. 2015, *MNRAS*, 454, 2787
- Hermes, J. J., Mullally, F., Østensen, R. H., et al. 2011, *ApJL*, 741, L16
- Hermes, J. J., Kepler, S. O., Castanheira, B. G., et al. 2013, *ApJL*, 771, L2
- Kepler, S. O., Castanheira, B. G., Saraiva, M. F. O., et al. 2005, *A&A*, 442, 629
- Kuschnig, R., Weiss, W. W., Gruber, R., Bely, P. Y., & Jenkner, H. 1997, *A&A*, 328, 544
- Landolt, A. U. 1968, *ApJ*, 153, 151
- Luo, A.-L., Zhang, H.-T., Zhao, Y.-H., et al. 2012, *RAA*, 12, 1243
- Mukadam, A. S., Montgomery, M. H., Winget, D. E., Kepler, S. O., & Clemens, J. C. 2006, *ApJ*, 640, 956
- Nather, R. E., Winget, D. E., Clemens, J. C., Hansen, C. J., & Hine, B. P. 1990, *ApJ*, 361, 309
- Rebassa-Mansergas, A., Liu, X.-W., Cojocaru, R., et al. 2015, *MNRAS*, 450, 743
- Ren, J., Luo, A., Li, Y., et al. 2013, *AJ*, 146, 82

- Ren, J. J., Rebassa-Mansergas, A., Luo, A. L., et al. 2014, *A&A*, 570, A107
- Su, J., Li, Y., Fu, J.-N., & Li, C. 2014a, *MNRAS*, 437, 2566
- Su, J., Li, Y., & Fu, J.-N. 2014b, *NewA*, 33, 52
- Tremblay, P.-E., Gianninas, A., Kilic, M., et al. 2015, *ApJ*, 809, 148
- Voss, B., Koester, D., Østensen, R., et al. 2006, *A&A*, 450, 1061
- Voss, B., Koester, D., Østensen, R., et al. 2007, 15th European Workshop on White Dwarfs, 372, 583
- Winget, D. E., & Kepler, S. O. 2008, *ARA&A*, 46, 157
- Winget, D. E., van Horn, H. M., Tassoul, M., et al. 1982, *ApJL*, 252, L65
- Zhang, Y.-Y., Deng, L.-C., Liu, C., et al. 2013, *AJ*, 146, 34
- Zhao, G., Zhao, Y.-H., Chu, Y.-Q., Jing, Y.-P., & Deng, L.-C. 2012, *RAA*, 12, 723
- Zhao, J. K., Luo, A. L., Oswalt, T. D., & Zhao, G. 2013, *AJ*, 145, 169